Proceedings of ALGORITMY 2002
pp. 1–12

DIRECT AND INVERSE SOLUTIONS OF THIN FILM FLOW PROBLEMS

GÜNTER BÄRWOLFF *

Abstract. The thin film flow between a magnetic head slider and a hard disk was described by a mathematic model based on the compressible Navier-Stokes equation. The assumption of a very small film thickness compared to the horizontal dimensions of the magnetic head slider leads to a 2d model - the Reynolds equation - for the computation of the pressure distribution beneath the slider. Both, direct and inverse problems are formulated. A mathematical analysis is done and a numerical model is constructed.
For the model validation flying height measurements in submicrometer range by means of white light interferometry were used with an assembly of equal magnetic disk sliders. Statistical evaluation shows reproducible deviations of steady–state flying characteristics from numerical calculations based on Reynolds equation with slip flow effect.
The basic discretisation principles of the mathematical model (direct and inverse problems) were demonstrated. Some aspects of grid generation and resulting difficulties were discussed and validated. In the result of the numerical calculations a proposal for an improvement of the white light measurement technique by a corrected color scale could be made. The corrected steady–state flying characteristics show an excellent agreement with calculations.

Key words. Convection-diffusion problem, thin film flow, mathematical and numerical analysis

AMS subject classifications. 35D05, 35J25, 35Q30, 35K57, 74S10, 76M12

1. Introduction. Magnetic disk sliders fly above high speed rotating disks using aerodynamic action. Present disk files operate with air film thickness of about or less then $0.2\mu m$ to assure a good recording density. Important tools of slider design are optical methods for flying height measurements and numerical air bearing calculation methods. Static flying height is usually measured by white light interferometry at a glass disk [1]. The resolution in the range of $0.1\mu m \ldots 1.0\mu m$ is determined as $0.05\mu m$. In [2] is shown that color tone depends on the slider material and light reflectivity of the surface. A photographic method is developed to achieve a higher resolution of $0.01\mu m \ldots 0.015\mu m$. For the validation of the mathematical and numerical model a work with a high resolution in visual observation is obtained by statistical methods [11]. Calculation results and measurement results are compared and differences are discussed.

2. Mathematical Model and Mathematical Analysis. The mathematical model to describe the steady–state flight of a slider (with a magnetic head) over a hard disk is based on the balances of mass and impuls of an air bearing. Under some special assumptions, like

– the flying height is small to be compared with the length of slider and
– the equation of state is of polytropic type,

we get from the compressible Navier–Stokes equation the Reynolds equation (dimensionless form) of the form

$$G\,\nabla\cdot(P^{1/n}H\cdot\vec{u}) = \nabla\cdot\left\{\frac{H^2}{M}P^{\kappa}(HP+6Kn_a)\nabla P\right\} \quad \text{in} \quad \Omega \quad . \tag{1}$$

*Technische Universität Berlin; email:baerwolf@math.tu-berlin.de

The equation (1) is valid in the air bearing, or more exactly, in the projection area of the slider rails Ω. In the mathematical model of the slider we consider for the inner and outer rail different velocities (u, v) depending on the local radius and yaw angle. If we suppose isothermic conditions, n and M are equal to 1 and from equation (1) follows

$$G\,(\vec{u}\cdot\nabla(HP)) = \nabla\cdot(H^2(HP+6Kn_a)\nabla P) \quad \text{in} \quad \Omega \quad , \tag{2}$$

for a constant velocity $\vec{u}$. At the boundary $\partial\Omega$ conditions of the form

$$P = 1 \quad \text{at} \quad \partial\Omega \tag{3}$$

are given. With the Knudsen number in the differential equation (1) we have considered "slip"–flow effects, that means the equation (1) describes also very thin flow films, in which the gas don't cling to a solid surface ($\vec{u} = 0$ is not given). The continuum hypothesis is valid only in the central region of the flow film. The solution and control of the boundary value problem (1),(3) is the essential basis to investigate the different problems of air bearing sliders. The mathematical analysis of the model and the construction of a numerical method for computation of the pressure field P and the hydrodynamic force w with the pressure center location (x_w, y_w) using the input informations of slider geometry, slider position (radius, yaw angle Φ), disc rotating number and slit geometry of air film, which is characterisized by h_m, α and β are the main goals. With $p = p_a P$ we get the hydrodynamic force w and its pressure center location from the following equation

$$w = \int_\Omega p\,d\Omega, \qquad x_w = \int_\Omega x(p-p_a)\,d\Omega, \qquad y_w = \int_\Omega y(p-p_a)\,d\Omega \tag{4}$$

The equation (2) is a nonlinear second order partial differential equation of convection–diffusion type. For the further investigations we write the equation (2) in the form

$$\vec{u}\cdot\nabla(H\overline{P}) - \nabla\cdot(\lambda(\overline{P}+1)\nabla\,\overline{P}) = f\ , \tag{5}$$

with

$$\lambda(P) = \frac{H^2}{G}(HP+6Kn_a) \qquad \text{and} \qquad f = -\vec{u}\cdot\nabla\,H\ .$$

Thus we have for $\overline{P}$ homogenous Dirichlet boundary data

$$\overline{P} = 0 \quad \text{at} \quad \partial\Omega\ . \tag{6}$$

For the qualitative analysis we modify the equation (5) in the following way. The coefficient λ of the equation will be substituted by the coefficient

$$\kappa_c = \frac{H^2}{G}(HP_a+6Kn_a) \geq \frac{h_m^2}{G}(h_mP_a+6Kn_a) =: c_\kappa = const.$$

with a mean pressure value P_a and thus the modified equation reads

$$\vec{u}\cdot\nabla(H\overline{P}) - \nabla\cdot(\kappa_c\nabla\overline{P}) = f\ . \tag{7}$$

This modification will be justified later. Now we will discuss existence and uniqueness results for the boundary value problem (7),(6).

THEOREM 2.1. *If* $ess\sup_\Omega(|\nabla\cdot(H\vec{u})|)$ *is small (small will be specified during the proof) and the velocity* $\vec{u}$ *is constant, then the boundary value problem (7),(6) has a unique weak solution* $\overline{P}\in H_0^1(\Omega)$.

Proof. The weak formulation of (7),(6) reads

$$a(\overline{P},Q) := \int_\Omega \kappa_c \nabla\overline{P}\cdot\nabla Q\,dF + \int_\Omega \vec{u}\cdot\nabla(H\overline{P})Q\,dF = \int_\Omega fQ\,dF\,, \tag{8}$$

and we have to find a $\overline{P}\in H_0^1(\Omega)$ for a given $f\in H^{-1}(\Omega)$.
$a(\cdot,\cdot)$ is a continuos bilinear form on $H_0^1(\Omega)$. Further we have

$$\int_\Omega (H\vec{u}\cdot\nabla\overline{P})\overline{P}\,dF = -\frac{1}{2}\int_\Omega \nabla\cdot(H\vec{u})\overline{P}^2\,dF\,.$$

With the inequality of Poincaré-Friedrichs

$$||\overline{P}||_{L^2}\le c_F||\nabla\overline{P}||_{L^2}$$

from the weak formulation we find

$$a(\overline{P},\overline{P}) \ge c_\kappa||\nabla\overline{P}||_{L^2}^2 + \frac{1}{2}\int_\Omega(\nabla\cdot(H\vec{u})\overline{P}^2\,dF$$

$$\ge c_\kappa||\nabla\overline{P}||_{L^2}^2 - \frac{c_F^2}{2}ess\sup_\Omega(|\nabla\cdot(H\vec{u})|)||\nabla\overline{P}||_{L^2}^2$$

and with the condition $ess\sup_\Omega(|\nabla\cdot(H\vec{u})|)\le const. < \frac{2c_\kappa}{c_F^2}$ we have

$$a(\overline{P},\overline{P})\ge c_\kappa||\nabla\overline{P}||_{L^2}^2\ a.e.,$$

that means $a(\cdot,\cdot)$ is strict positive on $H_0^1(\Omega)$. The lemma of Lax-Milgram guarantees the existence of a weak solution and from the above inequalities we see that the solution is unique. □

REMARK 2.2. *The condition*

$$ess\sup_\Omega(|\nabla\cdot(H\vec{u})|)\le const. < \frac{2c_\kappa}{c_F^2}$$

is for the given thin film flow problem realistic, because the ascent of the slider is very small (pitch, roll and taper angles are very small).
Now we will discuss the nonlinear problem with the coefficient

$$\kappa(\overline{P}) = \frac{H^2}{G}(H|\overline{P}+1| + 6Kn_a)$$

and thus we have the equation

$$\vec{u}\cdot\nabla(H\overline{P}) - \nabla\cdot(\kappa(\overline{P})\nabla\overline{P}) = f\,. \tag{9}$$

instead of the equation (5) or (7). We note that the equation (9) is our model equation (5) if $\overline{P}\ge 0$.

THEOREM 2.3. *If* $ess\sup_\Omega(|\nabla\cdot(H\vec{u})|)$ *is small and the velocity* $\vec{u}$ *is constant, then the nonlinear boundary value problem (9),(6) has a unique weak solution* $\overline{P}\in H_0^1(\Omega)$.

Proof. The proof is analog to the proof of theorem 2.1. We can show, that $\kappa(\overline{P})$ fulfills the conditions of lemma 1.6 of the book of Gajewski/Gröger/Zacharias [6] and

we have the strong monotonity of $a(\cdot,\cdot)$ and therefore the existence and the uniqueness of the solution. □

Now we will investigate if the solution $\overline{P}$ of the problem (9),(6) is non negative. We can show the

THEOREM 2.4. *If* $ess\sup_\Omega(|\nabla\cdot(H\vec{u})|)$ *is small,* $\nabla\cdot(H\vec{u})\leq 0$ *a.e. and the velocity* $\vec{u}$ *is constant, then the solution of the nonlinear boundary value problem (9),(6) is non negative.*

Proof. We take the weak formulation (8) with $Q=\overline{P}^-$ and get

$$\int_\Omega \kappa(\overline{P}+1)\nabla\overline{P}\cdot\nabla\overline{P}^-\,dF+\int_\Omega(H\vec{u}\cdot\nabla\overline{P})\overline{P}^-\,dF+\int_\Omega(\vec{u}\cdot\nabla H)\overline{PP}^-\,dF=-\int_\Omega\vec{u}\cdot\nabla H\,dF\,.$$

Now we follow a technique used in [7]. Because of the relations

$$\nabla\overline{P}\cdot\nabla\overline{P}^-=\nabla\overline{P}^-\cdot\nabla\overline{P}^- \quad , \qquad (\vec{u}\cdot\nabla\overline{P})\overline{P}^-=(\vec{u}\cdot\nabla\overline{P}^-)\overline{P}^- \quad , \qquad \overline{PP}^-=(\overline{P}^-)^2$$

we get

$$\kappa_1||\nabla\overline{P}^-||^2_{L^2}+\frac{1}{2}\int_\Omega\nabla\cdot(H\vec{u})(\overline{P}^-)^2\,dF+\int_\Omega(\vec{u}\cdot\nabla H)\overline{P}^-\,dF\leq 0\,,$$

with $\kappa_1=\frac{H^2}{G}6Kn_a$. Further we have $\vec{u}\cdot\nabla H=\nabla\cdot(H\vec{u})\leq 0$ because of the constance of $\vec{u}$. Then with the smallness of $ess\sup_\Omega(|\nabla\cdot(H\vec{u})|)$ we get the inequality

$$||\nabla\overline{P}^-||^2_{L^2}\leq 0$$

and this means $\nabla\overline{P}^-$ and $\overline{P}^-$ are equal to zero and thus $\overline{P}$ is a.e. non negative . □

With the theorem 2.4 we have shown the existence of the original mathematical model (5),(6). This justifies the use of $\kappa(P)$ instead of $\lambda(P)$.

REMARK 2.5. *The condition* $\nabla\cdot(H\vec{u})\leq 0$ *is valid for the considered slider configuration, because the velocity components are positiv and the* $\frac{\partial H}{\partial x}$ *is negative and* $|\frac{\partial H}{\partial y}|$ *is very small compared to* $|\frac{\partial H}{\partial x}|$.

3. Numerical Model for the Direct and Inverse Problem. Because of the fluid-aerodynamical background we prefer for the numerical solution of the boundary value problem a finite volume method (see [9]). The integration region Ω is discretisized by a grid of rectangles. The equation (1) is integrated over Ω. Using the additivity of the integral with respect to the integration region and the integral theorem of Gauss we get for all grid cells ω_{ij} (see 1) with the boundary γ the relation

$$\int_\gamma \vec{u}\cdot\underline{n}\,HP\,d\gamma+\int_\gamma\lambda(\nabla P)\cdot\underline{n}\,d\gamma=0 \tag{10}$$

where λ stands for the expression $H^2(HP+6Kn_a)/G$ and $\vec{u}=(u,v)=(cos\Phi,sin\Phi)$ is set for simplification. $\underline{\mathrm{n}}$ denotes the outer normal vector.

The analysis of the integral relation (10) for every cell yields under the assumption that the solution between two neighbouring cell centers can be approximately described by a piecewise linear function the following finite difference expression for the second integral

$$\begin{aligned} D_1=&(\lambda_{i+1/2j}(P_{i+1j}-P_{ij})/\Delta x-\lambda_{i-1/2j}(P_{ij}-P_{i-1j})/\Delta x)\Delta y\\ &+(\lambda_{ij+1/2}(P_{ij+1}-P_{ij})/\Delta y-\lambda_{ij-1/2}(P_{ij}-P_{ij-1})/\Delta y)\Delta x \quad . \end{aligned} \tag{11}$$

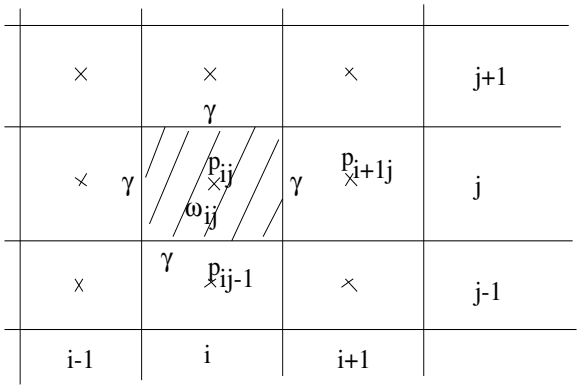

FIG. 1. *Cells and supporting points of finite–volume grid*

In the case of the convective terms (first integral of (4)) for P on the boundary γ of a cell we use a very special interpolation depending on the sign of u resp. v instead of the linear interpolation of the P–values in the centers of neighbouring cells to get a stable scheme. This interpolation gives us the weighted upwind approximation of the form

$$D_2 = (0.5(u-\tau|u|)(HP_{i+1j}-HP_{ij})/\Delta x + 0.5(u+\tau|u|)(HP_{ij}-HP_{i-1j})/\Delta x \\ +0.5(v-\tau|v|)(HP_{ij+1}-HP_{ij})/\Delta y + 0.5(v+\tau|v|)(HP_{ij}-HP_{ij-1})/\Delta y)\Delta x\Delta y \quad . \tag{12}$$

We have to choose the weighting factor τ from the intervall [0,1] in dependence of the magnitude of the bearing number G as small as possible, because the used approximation of the convective terms is of the order $O(h^{2-\tau})$.
For a transparent deduction of the difference expressions D_1 and D_2 we use a grid with the uniform grid parameters Δx, Δy and we suppose a piecewise constant velocity (u,v) with regard to the cells.
The result of the described integral–interpolation method is after addition of D_1 and D_2 and some simple steps of recalculation the following finite difference equation system

$$(u(HP)^{\circ}_{x} + v(HP)^{\circ}_{y}) - ([\frac{\tau}{2}|u|\Delta x + \lambda_{i+1/2j}]P_x)_{\overline{x}} - ([\frac{\tau}{2}|v|\Delta y + \lambda_{ij+1/2}]P_y)_{\overline{y}} = 0, \tag{13}$$

where i and j are indices of inner points of Ω. The discretisized boundary conditions

$$P_{ij} = 1 \quad , \tag{14}$$

close the equation system (13), where i and j are indices of boundary points of $\partial\Omega$ (boundary of Ω). The algebraic equation system (13),(14) is nonlinear, because the coefficient λ depends on the solution P. We solve (13),(14) with an iteration method of Gauss–Seidel type. The equation (13) shows, that an artificial conduction term follows from the use of an approximation like (12) with a nonzero τ. Especially in the case of very large bearing numbers we can solve the equation system in a stable way only with a τ near by 1. To minimize the resulting discretisation errors we have to guarantee that the terms

$$\frac{\tau}{2}|u|\Delta x P_{x\overline{x}}\ ,\ \frac{\tau}{2}|v|\Delta y P_{y\overline{y}} \tag{15}$$

will be small. If the expressions $P_{x\overline{x}}$, $P_{y\overline{y}}$ of (15) are very small in a subset Ω_s of the integration region Ω, then the discretisation error which follows from the upwind approximation is neglectible, on the other hand we have to make Δx and Δy very small to decrease the errors. The expressions (15) are used as error indicators. The local evaluation of the expressions (15) show the necessarity of a local grid refinement at the position l_1 behind the trailing edge because of the large curvature of the pressure field and the boundary layer at the trailing edge in the back area of the slider. Only the grid refinement in x–direction is essential. In the y–direction an equidistant grid is sufficient.

The validation of the numerical method was made by comparison of numerical results and experimental data from our laboratory (see [10]) of some well investigated flights of a winchester slider. Furthermore we compared our results successfully with the results of [2]–[8]. The numerical results presented in this paper we have got with a grid of 210 $\times$ 20 points for the discretisation of one slider rail (the bearing numbers amount approximately to 10^2 up to 10^5). This number of grid points was necessary to get a good coincidence (that means, that the differences of numerical and experimental results are less than accuracy of measurements). Also we have done computations with finer grids and thus we could show grid-independence of the results.

With the just described numerical solution method we are able to solve P, w, x_w and y_w for given h_m, α and β, that means direct problems. The computation of w, x_w and y_w after (4) is made analytically on the assumption that the solution of (13),(14) is piecewise linear.

The inverse problem means the computation of h_m, α and β from the solution of an equation system of the form

$$\begin{aligned} g_1 &= w(h_m,\alpha,\beta) - f = 0 \\ g_2 &= w(h_m,\alpha,\beta)(x_f - x_w(h_m,\alpha,\beta)) - m_\alpha = 0 \\ g_3 &= w(h_m,\alpha,\beta)(y_f - y_w(h_m,\alpha,\beta)) - m_\beta = 0\ . \end{aligned} \tag{16}$$

We use a Newton iteration method to solve this problem. Because the functional relations between w, x_w, y_w and h_m, α, β are not given explicitly, but only given implicitly over the boundary value problem (1),(3), we approximate the derivatives in the Jacobian of the Newton method by finite difference expressions, for example

$$\frac{\partial g_1}{\partial \alpha} \qquad \text{by} \qquad \frac{w(h_m,\alpha+\Delta\alpha,\beta) - w(h_m,\alpha,\beta)}{\Delta\alpha}$$

Following this, one Newton–iteration step for solving the equation system (16) requires the solution of four boundary value problems of type (1),(3). Additionally we have to solve the boundary value problem (1),(3) for the new Newton–iteration h_m^*, α^*, β^* to measure the quality. Using the fact, that the moments m_α and m_β in most of the practical problems are neglectible, we are able to consider the simplified system

$$\begin{aligned} e_1 &= w(h_m,\alpha,\beta) - f = 0 \\ e_2 &= x_f - x_w(h_m,\alpha,\beta) = 0 \\ e_3 &= y_f - y_w(h_m,\alpha,\beta) = 0 \end{aligned} \tag{17}$$

instead of the equation system (16) and we get a substantial simplification of the Jacobian. In addition to the determination of the steady–state flying parameters h_m, α and β with a Newton method following [11] we build the approached analytical relations of the form

$$h_m = a_1 * w^{b_1} * x_w^{c_1} * y_w^{d_1} \quad \alpha = a_2 * w^{b_2} * x_w^{c_2} * y_w^{d_2} \quad \beta = a_3 * w^{b_3} * x_w^{c_3} * y_w^{d_3} \tag{18}$$

with means of least square analysis. If we don't have any practical or experimental informations we can use the relations (18) to get a good start iteration for the Newton method, for example

$$h_m^0 = a_1 * f^{b_1} * x_f^{c_1} * y_f^{d_1}$$

etc.. The figures 2 and 3 show the pressure contour lines and the pressure mountain beneath the slider for $w = 150\,mN$ located at the geometrical center of the slider and $h_m = 165\,nm$, $\alpha = 12,9$" and $\beta = 3,7$" ($G = 3000$ (inner rail), $U = 20\,\frac{m}{s}$, $\Psi = 0$).

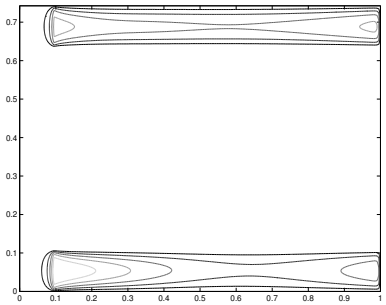

FIG. 2. *pressure contour lines*

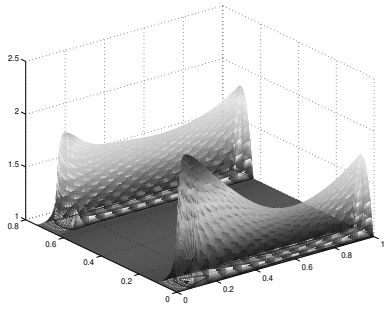

FIG. 3. *pressure mountain*

4. Slider Specifications and Physical Situation. Taper flat sliders made of AlTiC were used for this investigation. Table 1 shows the air bearing geometry and slider parameters (see fig. 4).

geometry	l_x	$4.00mm$
	b	$0.50mm$
	b_a	$2.20mm$
	l_1	$0.375mm$
	γ	45‘
	x_f	$2.00mm$ from leading edge
	y_f	symmetrical
material	slider suspension	3380 type
location at glass disk	Φ	0^o at pivot point
	r	$34mm \ldots 62mm$ at pivot point
	rotational speed of disk	$3740rpm$
	surface velocity U	$13.3m/s \ldots 24.3m/s$

TABLE 1
Slider configuration

A series of 27 sliders with an averaged slider load $w = 145mN$ and a deviation of $8mN$ rms was considered.

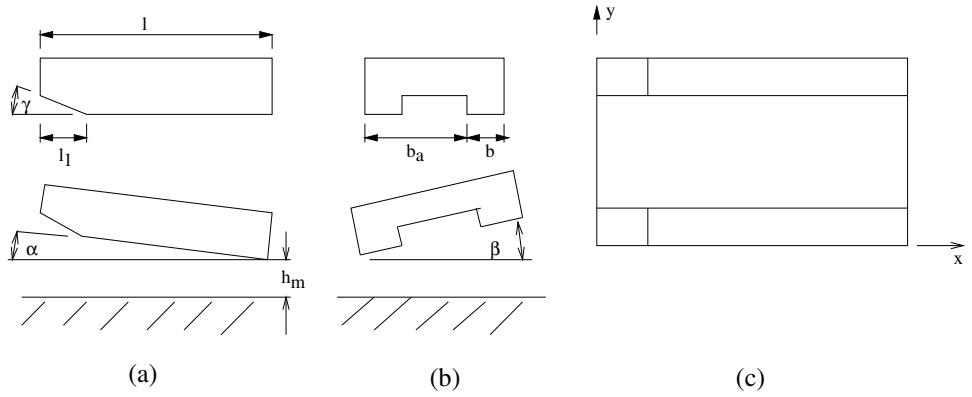

FIG. 4. *Slider specification, (a) side view, (b) back view, (c) view from below*

5. Numerical vs. Experimental Results. Flying height was measured by white light interferometry through a glass disk of 3 mm thickness. The white light source was a microscopy lamp (metal filament) with a day light filter. The optical system was used with magnification 25×, numerical aperture 0.08 and angle of incidence 20^o. The colors were determined visually at the four ends of the slider rails (at the centre lines; taper ignored). The flying height was found based on the color scale in [1], fig. 5. This color scale is listed in table 2, first and second column.

5.1. Results with the color scale of [1]. The flying height of a series of sliders were averaged. The mean deviations mainly caused by tolerances of the various sliders and color detection errors were $0.025\mu m$ rms at trailing edge and $0.05\mu m$ rms at leading edge for both series.
Results are plotted in fig. 5. H_o and H_i are spacing at leading edge (at the location $x = l_1$, $y = b/2$ resp. $y = b_a + b/2$), outer and inner rail, h_o and h_i are the same at trailing edge (at the location $x = l$, $y = b/2$ resp. $y = b_a + b/2$).
Fig. 5 shows that the flying height dependence on velocity determined by color scale [1] does not agree with calculation in this paper and in [2] – [8]. The measured curves have points of inflexions and regions with the false sign of curvature. It is found that near $0.2\mu m$ and $0.4\mu m \ldots 0.45\mu m$ the slope of the curves is too flat, but in the regions $0.25\mu m \ldots 0.35\mu m$ and $0.5\mu m \ldots 0.6\mu m$ too steep. Therefore the color scale for this special experimental apparatus must be corrected. Thus the influence of the color tone caused by material and reflexivity of the surfaces, the personal color sensitivity of the observer and the characteristics of the white light source were eliminated for visual observation.

5.2. Correction of Color Scale and Conclusional Results. Sliders of high flatness ($< 15nm$) were used to correct the color scale. 22 series of color location measurements along the slider rails were made with the slider in various static flying positions or resting in contact with an optical flat. The color locations we measured by an eyepiece screw micrometer.
The data of each slider position alone were fitted by linear regressions with the corresponding values from the color scale [1]. The achieved results from all slider positions for each color differed within $\pm 0.015\mu m$ and were averaged. The results reduced to 0^o incidence angle are listed in table 2, column 3. This color scale is used to plot the flying height of the above two series of sliders in fig. 6. These static flying character-

color	spacing (μm) found in [1]	spacing (μm) found in this work
very black	0.01	
black	0.03	
gray	0.05	
white	0.13	0.13
yellow	0.18	0.19
orange	0.20	0.21
red	0.23	0.24
violet	0.28	0.27
indigo	0.31	0.30
blue	0.35	0.32
green	0.38	0.36
yellow	0.41	0.42
orange	0.43	0.45
bright red	0.46	0.48
scarlet	0.49	0.51
purple	0.53	0.53
indigo	0.55	0.54
blue	0.59	0.56
green	0.63	0.60
yellow	0.68	
red	0.73	

TABLE 2
color scales for vertical incidence

istics are in better agreement with results of the calculation method described in this paper. The comparisons are demonstrated in fig. 7. They continously have negative curvature and no point of inflexion. To get one (h_m, r)–graph we have to solve six inverse problems for the radii $r = 35mm,\ 40mm,\ 45mm,\ 50mm,\ 55mm,\ 60mm$. The solution of an inverse problem needs two or three iteration steps (if the initial values of h_m, α and β are not very bad) to get an accuracy of 0.1 % with regard to the solution quality functional (for the case $m_\alpha = m_\beta = 0$)

$$Z(h_m, \alpha, \beta) = \frac{1}{3}[c_x(x_w - x_f)^2 + c_y(y_w - y_f)^2 + c_k(w - f)^2] \quad ,$$

with $c_x = 1/x_f^2, c_y = 1/y_f^2$ and $c_k = 1/f^2$.
At our numerical calculations we can't consider the torques m_α and m_β, because we have not reliable informations about these parameters. Nevertheless the consideration of a torque m_α of $12mN * mm$ leads to a h_m–increasing of nearly $10nm$ and an α–decreasing of nearly 1.5".
The calculated roll angles are in a sufficient coincidence with the experimental data, that means the differences between numerical and experimental data are 0.5" in maximum.

6. Conclusions. It could be shown that the boundary value problem (1),(3) has at least one weak solution P greater or equal to the Dirichlet boundary value 1. The discussed mathematical model and especially the inverse problem namely the equation system (16) with the boundary value problem (1),(3) as a restriction gives a very good possibility to solve problems of practical interest effectivly and accurately. With

regard to numerical solution of the problem (1),(3) by the described finite volume method the regions of large pressure curvatures and the boundary layer in the back area of slider require a solution adaptiv grid refinement.
The using of local variable velocities (at least in x–direction as a function of the radius and the yaw angle at the point (x, y) of Ω) along the rails gives better results than the using of constant averaged velocities for every rail. In disk regions with a small radius the using of variable velocities will be necessary.
The comparison of experimental results by white light interferometry using the corrected color scale and the numerical results of ourself and other In the case of our regular slider with two rails the finite volume method is good and flexible enough for the numerical solution of the boundary value problem (1),(3). The flying heights discussed in this paper were choosed because of the considered measurement technique and the mathematical and numerical model is only restricted by the continuum hypothesis i.e. the validity of the Reyolds equation. Thus the method is applicable to smaller flying heights. To illustrate this the figure 8 shows the computational results for $h_m = 140\,nm$, $\alpha = 7.6''$ and $\beta = 1,7''$ with $w = 280\,mN$ at the slider center($\Psi = 0$, $U = 20\,\frac{m}{s}$) of the investigated slider characterized in table 1.

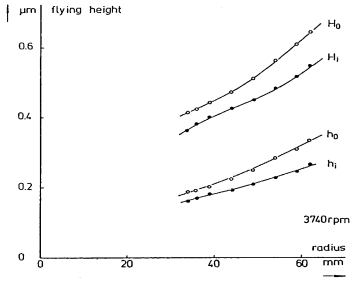

FIG. 5. *Experimental results with the color scale finding in [1]*

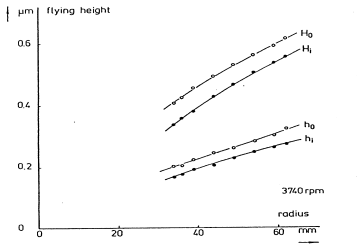

FIG. 6. *Experimental results with the corrected color scale*

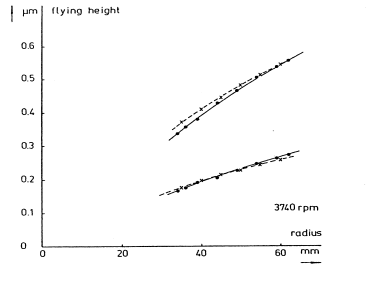

FIG. 7. *Comparison of experimental results with the corrected color scale and theoretical results for h_i and H_i, • experimental data, × numerical data (solution of inverse problems)*

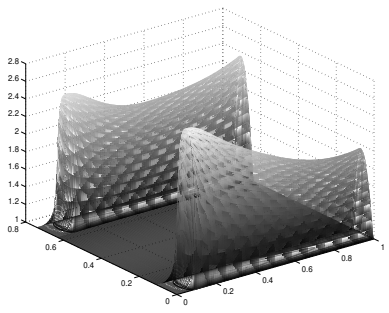

FIG. 8. *pressure mountain*

If the projection area Ω of the slider is more complex ("tripad–slider", "delta–slider", several types of zero–load–sliders) we have to work with appropriate finite cells ω_{ij} for the construction of a numerical solution of the boundary value problem (1),(3) instead of the rectangular finite volumes presented in this paper. Another possibility for the construction of a numerical solution method is the use of a FE-method based on the weak formulation (8).
In our solution procedure of the inverse problem we have to replace only the modular finite volume solver by a modified solver for the boundary value problem (1),(3) for a more complex region Ω.
The developed mathematical model and the numerical solution methods of the nonlinear direct and inverse problems allows both the efficient computation of a pressure field and the determination of the slider position (h_m, α and β) for a given load w and a pivot point (x_f, y_f) in a few seconds on a personal computer in a good quality compared to the experimental data.
For flying height in the range of about $20\,nm$ to increase the capacity of harddisks a description of the thin film flow by a Reynolds-type equation is possible, but hte equation has to be modified (see [12]). The presented mathematical and numerical considerations are still applicable.
But for a more precise description of the thin film flow problem the Boltzmann equation is much more suitable then Reynolds-type equations.

Acknowledgments. This paper was impossible without the very close cooperation to the engineer Christian Werner, who was responsible for the experimental data. He has also suggested the correction of the color scale of the white light interferometry and I have to thank him very hearty.

REFERENCES

[1] C. Lin and R. F. Sullivan, An Application of White Light Interferometry in Thin Film Measurements, IBM J. Res. Dev., Vol. 16, No. 3, 1972, pp. 269-276
[2] Y. Mitsuya and R. Kaneko, Molecular Mean Free Path Effects in Gas Lubricated Slider Bearings, Bull. JSME, Vol. 24, No. 187, 1981, pp. 236-242
[3] Yong Hu and D.B. Bogy, Solution of the Rarefied Gas Lubrication Equation Using an Additive Correction Based Multigrid Control Volume Method, Journ. of Trib., Vol 120, No. 2, 1998, pp. 280-288
[4] Y. Mitsuya, Thin Film Hydrodynamic Lubrication of lying Heads in Magnetic Disk Storages, Tribology international, Vol. 20, No. 6, 1987, pp. 322-330
[5] J.W. White, A Uniforma Flying Height Rotary Actuated Air Bearing Slider, IEEE Trans. Magn., Vol. Mag-22 No 5, 1986, pp. 1028-1030
[6] H. Gajewski, K. Gröger and K. Zacharias, Nichtlineare Operatorgleichungen und Operatordifferentialgleichungen, Akademie-Verlag Berlin 1974
[7] H. Gajewski, On iterative solution of nonlinear best-conduction and diffusion problems, Aplikace Matematiky (22)(1977), 77-91
[8] G. Bärwolff, Numerische Methoden zur Berechnung von Druckverteilungen und zur Identifikation von Luftlagern, Techn. Mech., 12(1991) Heft 1, pp. 1-5
[9] G. Bärwolff, Numerische Berechnung von Transportprozessen fluider Medien, ZWG/AdW–Report 2/88, Berlin 1988
[10] K. Graichen et al., Final Research Report about Aerodynamics of Magnetic Head Sliders (ZWG/AdW), Berlin 1988
[11] Chr. Werner, Internal Research Report of RED, Dresden 1986
[12] M. Anaya-Dufresne and G.B. Sinclair, Towards a Reyolds Equation for as Lubricated Bearings When Contact Occurs, Journal of Tribology, Vol. 124, April 2002, 266-273

Appendix.
$\vec{u} = (u, v)$ velocity vector related to surface velocity U at the slider center,

l_x characteristic length of air bearing (length of slider),
l_1 taper length,
γ taper angle,
b, b_a rail width, distance between rail centre lines,
r, Φ radius, yaw angle at the slider center,
$G = 6\frac{\mu_a l_x U}{p_a h_m^2}$ bearing number,
Ω projection area of slider rails,
μ, μ_a viscosity of air, characteristic viscosity of air (at ambient pressure p_a),
λ_a molecular mean free path (at ambient pressure),
$M = \frac{\mu}{\mu_a}$ dimensionless viscosity,
$Kn_a = \frac{\lambda_a}{h_m}$ Knudsen number,
$\kappa = (1-n)/n$ with polytropic exponent n,
h, h_m local film thickness, minimum film thickness (spacing, flying height),
α, β pitch and roll angle,
m_α, m_β impressed torques of slider in zero–position,
$H = H(x, y)$ normalized film thickness h/h_m,
$P = P(x, y)$ pressure field (related to ambient pressure)
w hydrodynamic force, load carrying capacity of bearing (two rails),
(x_w, y_w) pressure center location,
f slider load and
(x_f, y_f) location of pivot point.